Original Article

Evaluation of Antibacterial, Physicochemical, and Mechanical Properties of a Pit and Fissure Material Containing Silver Nanoparticles Attached to Metal-organic Framework

Niloofar Mokhtari [1]; Mahtab Memarpour [2]; Marzieh Alizadeh [2]; Azade Rafiee [2];

[1] Student Research Committee, School of Dentistry, Shiraz University of Medical Sciences, Shiraz, Iran.
[2] Oral and Dental Disease Research Center, Dept. of Pediatric Dentistry, School of Dentistry, Shiraz University of Medical Sciences, Shiraz, Iran.

KEY WORDS
Antibacterial;
Fissure sealant;
Mechanical properties;
Nanoparticles;

Received:
Revised:
Accepted:

ABSTRACT

Background: The use of nanotechnology in dentistry is considered as an innovative science to produce materials with more anti-caries properties. The release of metal ions and the longevity of the antibacterial activity of nanoparticles are critical factors that have garnered significant attention in recent research.

Purpose: The study compared the antibacterial effects, physicochemical, and mechanical properties of a resin -based fissure sealant (FS) dental material, plus silver (Ag) nanoparticles (NPs) doped copper-based metal-organic framework NPs (Ag@HKUST-1) to FS alone.

Materials and Method: HKUST-1 and Ag@HKUST-1 were characterized by Fourier transform infrared spectroscopy (FTIR), X-ray diffraction (XRD), Scanning electron microscopy (SEM), energy-dispersive X-ray spectroscopy (EDS), and Dynamic light scattering (DLS). Then, 0.1%, 0.5%, and 1% Ag@HKUST-1 plus a FS (Clinpro^{TM}, 3M, USPE, USA) compared to FS alone (control group). The antibacterial effects against *Streptococcus mutans (s. mutans)* were assessed with confocal laser scanning microscopy (CLSM), colony-forming unit (CFU) analysis, and SEM. Metabolic activity and cytotoxicity were evaluated by MTT assay and SEM.

Results: The results confirmed the successful synthesis of HKUST-1 and Ag@HKUST-1. Compared to control, the Ag@HKUST-1 + FS groups significantly reduced bacterial growth (p Value < 0.001). Both 0.5% and 1% Ag@HKUST-1 + FS groups had nonsignificant lower biocompatibility than the control group (p> 0.05). Based on the results, we selected the 0.5% Ag@HKUST-1 + FS group. The 0.5% Ag@HKUST-1 + FS group did not reduce shear bond strength, microleakage, or increase color change compared to the control (all p> 0.05). Depth of cure, microhardness, flowability, and flexural strength in the 0.5% Ag@HKUST-1 + FS group were higher than the control (all p< 0.05). The release of copper (Cu) ions increased between days 4–60, and Ag ions increased between days 1–21 and 30–60.

Conclusion: The antibacterial, physicochemical, and mechanical properties of 0.5% Ag@HKUST-1 + FS showed that it might be suitable alternative to conventional FS.

Corresponding Author: Memarpour M, Oral and Dental Disease Research Center, Dept. of Pediatric Dentistry, School of Dentistry, Shiraz University of Medical Sciences, Shiraz, Iran. Tel: +98-713-6263193-4
Fax: +98-713-6270325 Email: memarpour@sums.ac.ir

Cite this article as:

Introduction

Pit and fissure sealants materials (FS) are a preventive approach to reduce dental caries. The success of these treatments is attributed to an increased micromechanical

bond between FS and the enamel that promotes treatment longevity and effectiveness, and less biofilm formation on the FS surface, which decreases the risk for secondary caries [1-2]. Research recommends adding antibacterial agents or nanoparticles (NPs) to FS to minimize these risks [3-4].

NPs, which range in size from 0.1 to 100 nm, are used to improve the biomechanical and antimicrobial properties of dental materials [5]. The remineralization or antibacterial properties of the FS are increased by incorporating NPs during or before application of FS. These new materials have comparable physical properties to FS. The most common NPs used in dental materials are calcium phosphate, zinc oxide, and nanohydroxyapatite [3-4, 6]. Metal- and metal oxide-based NPs are used in dentistry because of their biocompatibility, and biological and antimicrobial activities. Inorganic metal compounds such as gold, silver (Ag), zinc, and copper (Cu) are frequently used for their antimicrobial properties [5]. The results of a study showed the antibacterial effects of FS that contain NPs, including Ag NPs. These materials have a superior performance in terms of antimicrobial activity compared to conventional FS [7]. A study reported the benefits of Cu NPs to enhance the physical, chemical, and antimicrobial properties of various dental materials [8].

The purpose of this study was to develop a new FS doped copper-based metal-organic framework (MOF) NPs (HKUST-1) for loading Ag NPs, which we named Ag@HKUST-1. The HKUST-1 and Ag@HKUST-1 were characterized by laboratory analyses. Moreover the study aimed to prepare different concentrations of the NPs to evaluate its cytotoxicity and antibacterial effects against *Streptococcus mutans* (*S. mutans*), and subsequently to select the most effective concentration of Ag@HKUST-1 for additional assessment. The antibacterial effects, and physicochemical, and mechanical properties of the selected NP-FS were then supposed to be compared with FS without NPs, as the control group. Hence, the null hypothesis was that the mentioned properties would not differ between the FS with and without NPs.

Materials and Method

Preparation of HKUST-1 and Ag@HKUST-1 nanoparticles (NPs)

HKUST-1 NPs were synthesized by the hydrothermal method. Initially, 1,3,5-benzenetricarboxylic acid (0.34 g, 1.6mmol) and Cu II nitrate trihydrate (1.3g, 5.35 mmol) were dissolved in 15ml of deionized water (DW) and stirred for 15 min. The solution was autoclaved at 80°C for 24 h. The suspension was cooled, centrifuged (4000 rpm, 10 min), washed three times with DW/pure ethanol (2:1), and dried in a vacuum oven (24 h, 60°C) [9-10]. We prepared the Ag@HKUST-1 by adding 150mg of silver nitrate to a suspension of HKUST-1 in DW. This mixture was continuously ultrasonicated for 30 min and then transferred to a stainless-steel autoclave (160°C, 12h). The suspension was cooled, washed, and dried as previously described [11-12]. HKUST-1 and Ag@HKUST-1 were characterized by the following tests.

Fourier transform infrared spectroscopy (FTIR)

Fourier transform infrared spectroscopy (FTIR) was used to assess the functional groups of HKUST-1. A vortex instrument (Vortex, Bruker, Germany) was used to collect the spectra over 4000–500 cm^{-1} at 8 cm^{-1} resolution with an average of 256 scans. FTIR also assessed ag@HKUST-1.

X-ray diffraction (XRD)

The HKUST-1 and Ag@HKUST-1 NPs were assessed by X-ray diffraction (XRD, D8 Advance, Bruker, Germany) at 40 kV and 40 mA using Cu Kα radiation. A total of 2g of the powder was scanned over a range of angle 2θ =5°–80° at a step size of 0.02° and time per step of 2 s.

Scanning electron microscopy (SEM) and energy-dispersive X-ray spectroscopy (EDS)

We evaluated the three-dimensional structure and morphology of the HKUST-1 and Ag@HKUST-1 NPs by scanning electron microscopy (SEM, TESCAN-Vega 3, Czech Republic) at a magnification 5000X–15 000X and 20 kV. The elemental mapping of Ag@HKUST-1 was assessed using energy-dispersive X-ray spectroscopy (EDS).

Dynamic light scattering (DLS)

We mixed 10mg each of the HKUST-1 and Ag@HKUST-1 NPs in 1 mL of DW to measure their sizes with a dynamic light scattering (DLS) device (SZ-100, Horiba, Japan).

Early experimental groups (0.1%, 0.5%, 1.0% Ag@HKUST-1+FS)

A common resin-based FS (Clinpro, 3M, ESPE, USA) was used in all the experimental groups. The Ag@HKUST-1 NPs were mixed with FS at the following weight

concentrations: 0.1 weight % (wt.%), 0.5 wt.%, and 1.0 wt.% to create the following experimental groups: 0.1%, 0.5%, and 1.0% Ag@HKUST-1+ FS. All groups underwent cytotoxic, morphologic, and antibacterial assessments and were compared to a control group (FS without NPs).

Evaluation of antibacterial effect in the experimental and control groups

Bacterial culture and biofilm formation

S. mutans (TCC 164, 99.7.13, IROST, Tehran, Iran) was cultivated in Brain Heart Infusion culture medium. A 1% inoculum of the bacterial suspension was added to the medium and incubated for 24 h at 37°C and 5% CO_2. Then, the optical density (OD) of the bacterial suspension was measured at 600 nm using a spectrophotometer (ELISA reader; Epoch, BioTek, USA) and adjusted to 2.5 McFarland [approximately 7.5×10^8 colony forming unit (CFU)/mL] with broth culture medium to form the inoculation medium for the subsequent experiments [4, 13].

Confocal laser scanning microscopy (CLSM)

FS from the experimental and control groups were placed in a sterile 96-well plate (5 mm diameter, 1 mm height), with two replicates per well. The samples were cured using a light-curing unit (Coltolux II, Colten, USA) at 550mW/cm² and 1 mm distance for 60 s, and sterilized by a UV lamp. The samples were incubated at 37°C and 5% CO_2 for 24 h. Next, 100 µL of the inoculation medium was added and the suspension was cultured for an additional 24 h to form relatively mature biofilms on the resins. The samples were gently washed with phosphate-buffered saline (PBS) to remove loosely attached bacteria. In order to distinguish between live and dead bacteria, we stained the samples with Syto 9 and propidium iodide, respectively. Live bacteria stained with Syto 9 produced a green fluorescence, and bacteria with compromised membranes that were stained with propidium iodide produced a red fluorescence. The stained samples were observed under a confocal laser scanning microscope (CLSM; LSM 800, Carl Zeiss, Germany) and the images were captured [4, 14-15].

Colony forming unit (CFU) assay

The CFU test was used to evaluate the antibacterial effect of the NPs. Disc-shaped specimens were fabricated, and biofilms were formed by adding 100 µL of the inoculation bacteria medium to each well. The wells were incubated as previously explained. Next, 1mL of broth was added to each well, and the samples were subjected to ultrasound for 10 min to dislodge the biofilm from the surface. The resultant bacterial suspension was collected, and its OD was measured at 600 nm using a microplate reader (Epoch-2-Microplate, BioTek, USA) to estimate bacterial concentration. The bacterial suspension was then serially diluted (1/2, 1/4, 1/8, and 1/16), and 10 mL of each dilution was spread onto agar plates that contained 5% sheep blood (n= 4). The plates were incubated (37°C, 5% CO_2, 48 h) and the colony number was counted using a colony counter (SANA SL-902, IRAN). The experiments were performed in triplicate [4, 13].

Scanning electron microscopy (SEM) analysis

Bacterial morphology on the FS samples from all the groups were observed by SEM. Specimen-fabrication, bacterial inoculation and washing with PBS was performed as previously described (We placed a 2.5% glutaraldehyde solution into each well and allowed the wells to remain under a fume hood for one hour. Each well was rinsed with PBS followed by the addition of 2% osmium tetroxide for 30min. The solution was dehydrated in a graded ethanol solution (25%, 50%, 75%, and 100%) for 15min each. The infiltrated bacteria were effectively fixed and prepared for SEM assessment [4, 13].

Metabolic activity and cytotoxicity evaluation

The 3-(4,5-dimethylthiazol-2-yl)-2, 5-diphenyltetrazolium bromide (MTT) assay is a colorimetric assay that measures the enzymatic reduction of MTT, a yellow tetrazole to formazan. The biofilm metabolic activity and cytotoxicity of the materials on the bacteria were assessed using the MTT assay. After biofilm formation, 20µL of 0.5mg/mL MTT solution was added to replace 80µL of the culture medium in each well. The wells were incubated for 4 h to enable formazan crystal formation. Then, 200µL of dimethyl sulfoxide (DMSO) was added to solubilize the crystals. The discs were incubated for 20min in the dark at room temperature. Next, 200µL of the DMSO solution in each well was transferred to a new 96-well plate, and a microplate reader was used to measure absorbance at 570–600 nm.

A higher absorbance indicates a higher formazan concentration, which means a higher metabolic activity in the biofilm on the disk. Six replicates were tested for

each group (n= 4). The concentration-percentage graph was plotted to determine the concentration required to inhibit 50% of bacterial growth (IC50) [15-16].

Cell culture

Human gingival fibroblast cells (Geniranlab.ir) were used to evaluate cytotoxicity. The cells were initially cultured and maintained in Dulbecco's Modified Eagle's Medium supplemented with 10% fetal bovine serum, 1% L-glutamine, and 1% penicillin-streptomycin, and incubated in a humidified atmosphere (5% CO_2, 37°C). The cell flasks were checked daily under a light microscope to monitor cell growth. Upon observing sufficient proliferation, cell counting was performed using the trypan blue dye exclusion assay. A cell density of approximately 1×10^4 cells/mL was used for the cytotoxicity tests [4,16].

Cytotoxicity assessment

Disc shaped samples were prepared as described. A total of 10×10^4 cells/mL of human gingival fibroblast cells seeded onto each well and the plates were incubated at 5% CO_2 and 37°C for 72h. Then, 80mL of the cell culture medium was replaced with 20mL of the 0.5mg/mL MTT solution. DMSO was added and the absorbance was measured as explained before. The concentration-percentage of viable cells was calculated as follows[4, 16] (eq 1):

$$\%\, Viability = \left[\frac{(Sample\ Absorbance\ -\ PBS\ Absorbance)}{(Control\ Absorbance\ -\ PBS\ Absorbance)}\right] \times 100$$

The IC50 was also calculated.

Scanning electron microscopy (SEM) analysis

The polymerization, sterilization, and cell culture stages were performed as previously described.SEM was used to determine the cells that infiltrated into the samples. Preparation steps that included cell fixation and dehydration were performed as mentioned earlier.

Laboratory analysis of the fissure sealant (FS) properties in the 0.5% Ag@HKUST-1 + FS versus FS without NPs

The biocompatibility and antibacterial tests results indicated that 0.5% Ag@HKUST-1 was the FS that contained the most effective and lowest NPs. Therefore, we selected this group plus FS (FS + 0.5% Ag@HKUST-1) for additional experimentation compared to a control group (FS without NPs).

Depth of cure

The depth of cure of the groups was assessed according to ISO 6874. FS molds (4 mm diameter, 6 mm height) were prepared and light-cured for 30 s (n = 5 per group). The height of the cured material was measured in mm using a digital caliper (Shoka Gulf, Japan) and a dental explorer. The measurement was repeated three times for each sample in both groups [4,13].

Microhardness test

FS discs (6mm diameter, 3mm height) were prepared from both groups and light-cured for 30 s (n= 12 per group). The FS were removed from the molds and stored in DW (37°C, 24h). The Vickers microhardness number (VHN, MHV-1000Z, SCTMC, China) of the surface was measured by applying a 50 g force for 30 s on each sample [7,13,17].

Flowability

We separately placed 50 mL of each group on glass slides and covered each slide with another slide (n = 5 per group). A 150 g force was applied to the slide surface for 1 min. Next, we measured the diameter of the resin spread (mm) using a digital caliper. This measurement was repeated three times for each sample [13,17].

Flexural strength test

FS bars (24 mm length, 2 mm width, 2 mm height) were prepared from the experimental and groups and light-cured for 40 s (n= 12 per group). The FSs bars were stored in DW for 24 h. Flexural strength was measured using a Universal Instron Machine (Zwick-Roell, Zwick Ulm, Germany) at three points, at a 20 mm distance and a force rate of 0.5 mm per min. The results were recorded in megapascals (MPa) [3,4,13].

Shear bond strength (SBS)

A total of 30 permanent third molar teeth mold were prepared and randomly divided into two groups (n = 15 per group). The enamel surface of the teeth was etched with 37% phosphoric acid gel (ESPE, 3M, USA), washed, and dried (all 20 s). Cylindrical FS molds for both groups were prepared on the etched surfaces using plastic cylinders (3 mm diameter, 3 mm height). The cylinders were incrementally filled with 1 mm layers of FS and light-cured for 40 s for each layer. The prepared samples were stored under humid conditions for 24 h. The SBS test was performed using a Universal Instron Machine where a force was applied parallel to the bonding surface at a crosshead speed of 1 mm/min until failure. The results were recorded in MPa. [17]. The type of

surface failure was examined by two blinded observers using a digital microscope at 25× magnification and recorded as (1) adhesive failure at the junction of FS and enamel, (2) cohesive failure in the enamel or FS structure, and (3) mixed failure if both adhesive and cohesive failure were observed in the sample.

Microleakage test

We used 24 intact permanent third molar teeth for this assessment (n= 12 per group). After etching and drying the surface, the FS was placed on the occlusal surface and cured as previously described. The teeth underwent 1000 cycles between 2±5°C and 55±2°C in a water bath, with a dwell time of 30s and a 15s transit time between the baths. The apex of each tooth was subsequently sealed with adhesive wax, and all the root and crown surfaces, except for a 1mm margin around the FS, were covered with two layers of nail polish. The samples were then placed in 0.5% fuchsine solution (Merck, Darmstadt, Germany) for 24h, washed and sectioned in the buccolingual direction. The prepared sections were examined under a digital microscope at 50× magnification to assess the extent of microleakage. The microleakage ratio for each sample was obtained by dividing the amount of microleakage by the penetration depth of the FS and recorded in mm [18].

Color change measurement

A total of 24 intact third molar teeth were selected (n = 12 per group). After etching and drying the surface, we prepared a cylindrical mold by using a plastic cylinder (5 mm diameter, 2 mm height) as explained before. The color of the samples was measured in two stages: immediately after preparing the mold and after 5000 thermocycles as previously explained. A spectrophotometer (Minolta Chromameter CR-241, Minolta Camera Co., Osaka, Japan) was used to measure the color with a light beam diameter of 0.3 mm on a gray background. The L*a*b* (CIE) values were determined for each sample, and the measurement was repeated three times for each sample. The color difference of the experimental samples compared to the control group was calculated using the following equation. In this formula, ΔE is the amount of color difference, and ΔL*, Δa*, and Δb* indicate the change in brightness, red-green ratio, and blue-yellow ratio, respectively (L*=49.2, a*= -0.4, b*= 0.0).

$$\Delta E = \sqrt{(\Delta L^*)^2 + (\Delta a^*)^2 + (\Delta b^*)^2}$$

Release of silver (Ag) and Copper (Cu) ions

Two molds (12mm×2mm×2mm) for the experimental and control groups were prepared using compression silicone material (Speedex, Coltene, Switzerland). FS was injected into each mold and light-cured for 40 s. Each block was removed cured again for 40 s. Two blocks in each group were prepared (n= 2 per group) to evaluate the release of Ag and Cu ions. Each block was immersed in 16mL of DW, with a solution-to-sample volume ratio of 3mm³/mL. We assessed the amount of ions released into the solution by collecting 5 mL samples in falcon tubes 24h (day 1) after the blocks were immersed in DW. The blocks were stored in a refrigerator at 3–4°C. The remaining solution was discarded, and each block was placed in a new solution. Using the same method, 5mL samples were prepared from each falcon tube on days 2, 4, 21, 30, 60, and 90. The release rate of Ag and Cu ions was measured using an ICP-Mass device (Optima 8300, Perkin Elmer, USA) [4,13,17].

Statistical analysis

All quallatitive assays were performed and replicates as noted, and unpaired *t*-test was performed to investigate the significance. The compatible software generated the data for each test. The data for quantitative analyses were reported as the means ± standard deviation (SD) and were analyzed with SPSS version 22.0 (IBM SPSS, New York, USA) software. The microhardness, flexural strength and shear bond strength tests were assessed by one-way analysis of variance (ANOVA) and Tukey HSD post hoc test. Microleakage was compared by Kruskal–Wallis H test and Mann–Whitney U test. For all comparisons, *p* values less than 0.05 were considered statistically significant.

Ethics approval

The study was approved by the Ethics Review Committee of the School of Dentistry, Shiraz University of Medical Sciences (IR.SUMS.DENTAL.REC.1401.041).

Consent to participate

All methods were performed in accordance with the relevant guidelines and regulations (*Declaration of Helsinki*). Written informed consents for the use of the teeth were obtained from the participants.

Results

Characterization of HKUST1 and Ag@HKUST-1

The successful synthesis and structural integrity of the HKUST-1 and Ag@HKUST-1 crystals were confirmed

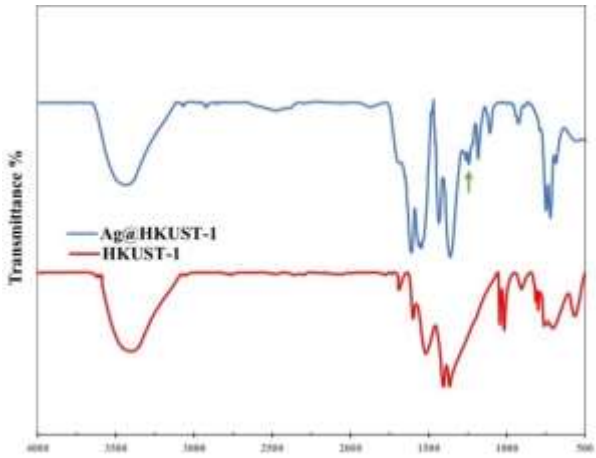

Figure 1: FTIR spectra of HKUST-1 and Ag@HKUST-1. Green arrow shows the Ag-O bond. FTIR: Fourier transform infrared spectroscopy; HKUST-1: Copper-based metal-organic framework (MOF) nanoparticles (NPs); Ag@HKUST-1: Silver (Ag) NPs attached to copper-based MOF NPs

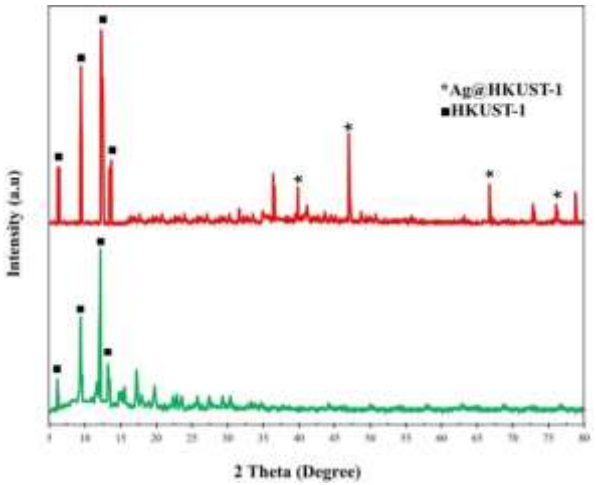

Figure 2: XRD pattern of the crystalline structures of HKUST-1 and Ag@HKUST-1. XRD: X-ray diffraction; HKUST-1: Copper-based metal-organic framework (MOF) nanoparticles (NPs); Ag@HKUST-1: Silver (Ag) NPs attached to copper-based MOF NPs

by FTIR spectroscopy, XRD, SEM, EDS, and DLS.

Fourier transform infrared spectroscopy (FTIR) analysis

Results of the FTIR spectra for the HKUST-1 functional groups (Figure 1) showed the peaks of the groups as follows: Cu-O bonds at 702 cm^{-1}, 1365 cm^{-1}, and 1404 cm^{-1} that corresponded to a C-O stretching vibration (H_3BTC). We postulated that the 1515^{-1} cm peak belonged to the C=C group, the 1599 cm^{-1} peak belonged to the C=O group of aromatic rings, and a broad peak at 3392 cm^{-1} represented the OH group. The bond at around 1246 cm^{-1} was presumed to represent Ag-O in the Ag@HKUST-1 group.

X-ray diffraction (XRD)

The XRD pattern of synthesized HKUST-1 was observed at 2□ values of 6.15°, 9.45°, 12.15°, and 13.2°, which corresponded to the (200), (220), (222), and (400) crystal planes of HKUST-1, respectively. Peaks at 39.91°, 47.32°, 66.71°, and 76.33° were related to the (111), (200), (220), and (311) crystal planes of the Ag NPs, respectively. All indicated a high degree of crystallinity for Ag@HKUST-1 (Figure 2).

Scanning electron microscopy (SEM) and energy-dispersive X-ray spectroscopy (EDS)

We observed a three-dimensional structure for HKUST-1 with a disordered octahedral form (hexagonal-like); this confirmed successful synthesis of the doped material (Figure 3a). SEM showed that the Ag@HKUST-1 nano cubes, which indicated successful loading of these had uniformly dispersed synthesized small spherical Ag NPs that were attached to the edge and vicinity of the NPs (Figure 3b). The EDS test was used to measure the chemical composition of the Ag@HKUST-1. The results showed the presence of carbon, oxygen, Cu, and Ag, and indicated high purity of the Ag@HKUST-1 (Figure 3c and d).

Dynamic light scattering (DLS) analysis

The average particle size of HKUST-1 was 295nm and the polydispersity index was 0.7. The Ag@HKUST-1 particle size was approximately 313 nm, which was consistent with the particle sizes measured by SEM (Figure 4).

Antibacterial effects

Confocal laser scanning microscopy (CLSM) analysis

CLSM was used to assess the viability of *S. mutans* biofilm on each sample. The images showed that the increased percentage of Ag NPs led to increased numbers of dead bacteria (Figure 5).

Colony forming unit (CFU) assessment

Although the control (FS) group showed a five-fold increase in bacterial growth after 48 h, the 0.1%, 0.5%, and 1.0% Ag@HKUST-1+FS groups had marked growth inhibition and bacterial death (Figure 6a). There was a significant difference between all groups ($p< 0.001$). The 1% Ag@HKUST-1+FS group had a 1.6-fold reduction in bacteria compared to the first day. Table 1 shows the two-day bacterial suspension concentrations for all groups after dilutions. The results of bacteria cou-nt on the surface of 5% blood agar plates after 48h showed that bacterial growth in the control (FS) group was high at all dilutions ($p< 0.001$) (Figure 6b and Table 2).

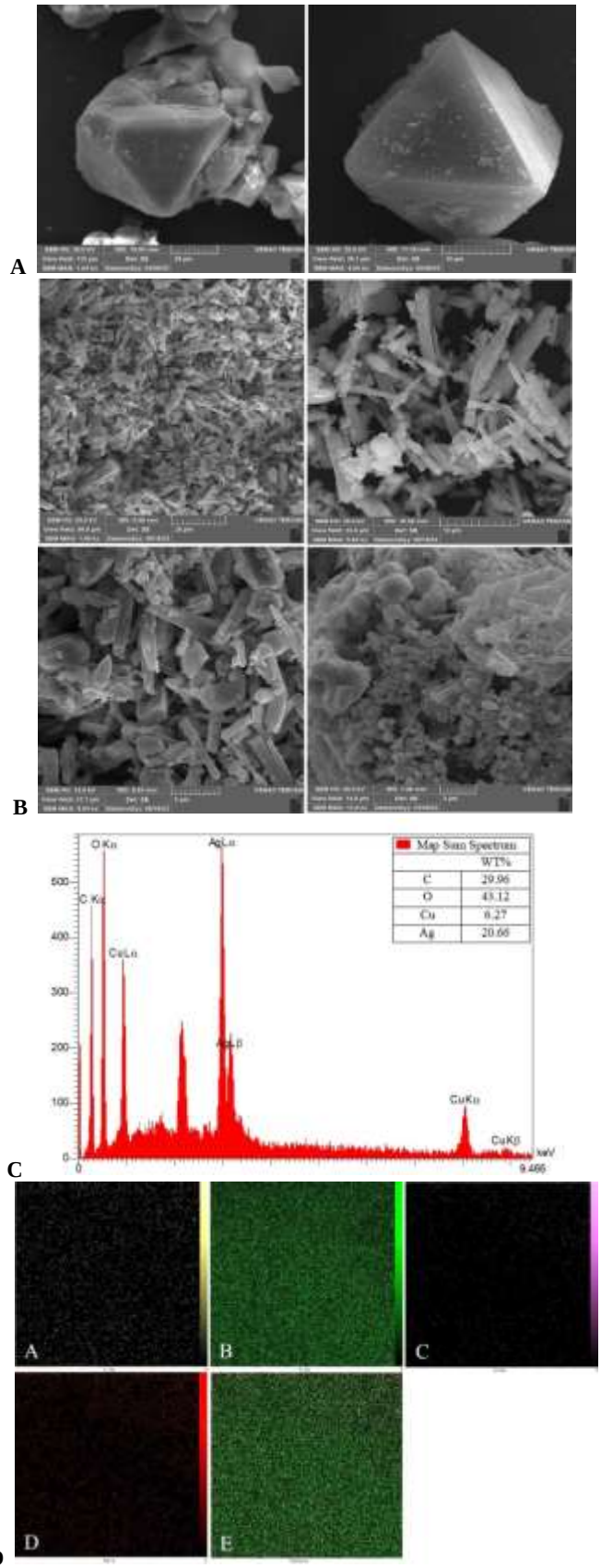

Figure 3: a: Three-dimensional SEM images of HKUST-1 in two different directions (magnification: 1640× and 4850×), **b:** Three-dimensional SEM images of Ag@HKUST-1 (magnification: 2000x and 13000x), **c:** EDS spectrum of Ag@HKUST-1 and wt.% of carbon, oxygen, Cu, and Ag in the NPs, **d:** Mapping of the elements in Ag@HKUST-1. **a:** Carbon, **b:** Oxygen, **c:** Cu, **d:** Ag, and **e:** Combination of the elements. HKUST-1: Copper-based metal-organic framework (MOF) nanoparticles (NPs); Ag@HKUST-1: Silver (Ag) NPs attached to copper-based MOF NPs; SEM: Scanning electron microscope; EDS: Energy-dispersive X-ray spectroscopy; wt.%: Weight percentage; NPs: Nanoparticles; Ag@HKUST-1: Silver (Ag) NPs attached to copper-based metal-organic framework (MOF) NPs; Cu: Copper

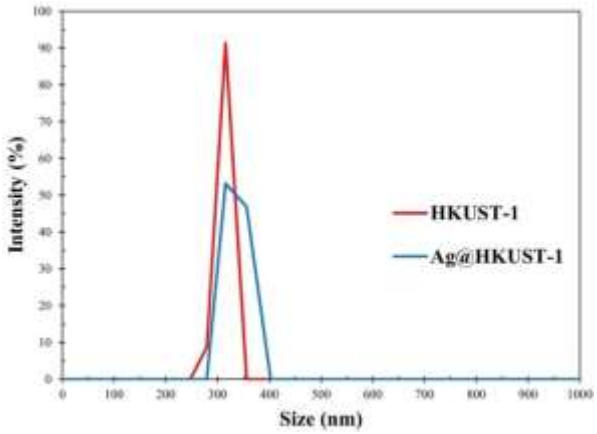

Figure 4: Graph of NPs from HKUST-1 and Ag@HKUST-1 detected by DLS. NPs: Nanoparticles; HKUST-1: Copper-based metal-organic framework (MOF) nanoparticles (NPs); Ag@HKUST-1: Silver (Ag) NPs attached to copper-based MOF NPs; DLS: Dynamic light scattering

The other groups demonstrated some degree of antibacterial and inhibitory effects ($p< 0.001$). There was a significant difference at all dilution-ns ($p< 0.001$), except for the FS+0.5% AgHKUST-1 and FS+1% Ag@-HKUST-1 groups ($p= 0.145$).

Scanning electron microscopy (SEM) analysis

Figure 7 shows the morphology and adhesion of *S. mutans* bacteria on the FS surfaces after 48 h. The control group (FS without NPs) displayed high numbers of dense elongated chains of diplococci bacteria. The antibacterial activity of all the experimental groups showed minimal or no bacterial adherence.

Metabolic activity and cytotoxicity

The viability of the *S. mutans* biofilm in the control FS without NP group was 100% (Figure 8). In contrast, the viability of bacteria the in 0.1%, 0.5%, or 1.0% Ag@H-KUST-1+FS groups were 35%, 28.5%, and 20.7%, respectively. We noted that the bacteria growth decreased significantly over time. The IC50 results indicated that the inhibitory effect of the bacteria was approximately 0.0002% by weight of these NPs in the FSs.

Cytotoxicity assessment

Cell viability in the negative control group (only living cells) was 100%, FS without NPs (control) was 92.95%, and the 0.1%, 0.5%, and 1% of Ag@HKUST-1 + FS groups were 136.77%, 96.52%, and 87.33%, respectively (Figure 9). The IC50 results indicated that up to 4.7% by wt% of the FS + NPs did not cause cell toxicity.

Scanning electron microscopy (SEM) analysis

SEM images of the control group (FS without NPs) showed a smooth, uniform surface while the 0.1%, 0.5% and 1.0% Ag@HKUST-1+FS groups all displayed a porous structure suitable for cell growth, adhesion, and biocompatibility. Cytotoxicity was not observed in the 1% Ag@HKUST-1 + FS group (Figure 10).

Fissure sealant (FS) properties

Depth of cure

The mean±standard deviation (sd) depth of cure in the 0.5%Ag@HKUST-1 group was 2.85±0.01mm, which was significantly greater than the control (FS without NPs) group (2.15±0.02mm) ($p= 0.001$). However, the average depths of cure of both groups were higher than the ISO standard (1.5 mm).

Microhardness test

The results of the microhardness values (VHN) showed that the mean±sd of the control (10.64±0.4) was significantly lower than the 0.5% Ag@HKUST-1 + FS group (13.9 ± 0.1) ($p= 0.0002$).

Flowability

The mean±sd of the 0.5% Ag@HKUST-1+FS group (4.23

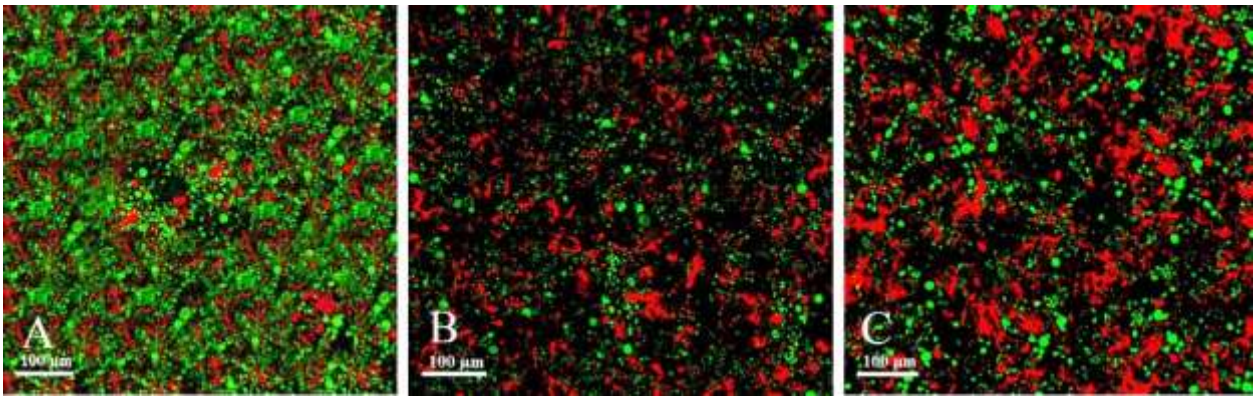

Figure 5: CLSM analysis of live (green) and dead (red) *Streptococcus mutans* (*S. mutans*) bacteria on the surface of the FS that contains: A)1% Ag@HKUST-1, B) 0.5% Ag@HKUST-1, and C) 0.1% Ag@HKUST-1. CLSM: Confocal laser scanning microscopy; FS: Fissure sealant; Ag@HKUST-1: Silver (Ag) nanoparticles (NPs) attached to copper-based metal-organic framework (MOF) NPs.

Table 1: Concentration of *Streptococcus mutans* (*S. mutans*) suspension after 48 h on the surfaces of the study groups

	FS	FS + 0.1% Ag@HKUST-1	FS + 0.5% Ag@HKUST-1	FS + 1% Ag@HKUST-1
CFU	$25 \times 10^8 \pm 0.4$	$11 \times 10^8 \pm 1.6$	$2 \times 10^8 \pm 0.4$	$3 \times 10^7 \pm 0.1$
1/2	12.55×10^8	5.8×10^8	1.15×10^8	1.5×10^7
1/4	6.27×10^8	2.9×10^8	5.7×10^7	7.5×10^6
1/8	3.13×10^8	1.45×10^8	2.8×10^7	3.7×10^6
1/16	1.56×10^8	7.25×10^7	1.4×10^7	1.7×10^6

FS: Fissure sealant; Ag@HKUST-1: Silver (Ag)-based nanoparticles (NPs) attached to copper-based. metal-organic framework (MOF) NPs; CFU: Colony forming unit

±0.01mm) was significantly more than the control group (2.17±0.05mm) (p= 0.005). According to ISO 6876 guidelines [19], the maximum acceptable number is 5mm.

Flexural strength test

The mean±sd flexural strength of the control group (58.7±3.9 MPa) was significantly lower than the 0.5% Ag@HKUST-1 + FS group (67.19±3.1 MPa) (p= 0.03).

Shear bond strength (SBS) test

There was no significant difference between the control (FS without NPs) group (14.60±0.3 MPa) and the 0.5% Ag@HKUST-1 group (14.48±0.8 MPa) (p= 0.18). Failure mode analysis revealed that cohesive and mixed fractures were the most frequent in both groups (Table 3).

Microleakage test

No significant difference was observed in microleakage between the control group (0.19±0.19mm) and the 0.5% Ag@HKUST-1+FS group (0.12±0.13mm) (p= 0.92).

Color change measurement

The mean values of ΔL and ΔE for the control group were (-11.95 to -10.20) 11.20 and (13.31 to 16.51) 14.87, respectively. The mean values of ΔL and ΔE for the 0.5% Ag@HKUST-1 + FS group were (-15.90 to -10.55) 10.80 and (14.49 to 16.66) 15.12, respectively. There were no significant differences between the groups for ΔL (p= 0.448) and ΔE (p= 0.649).

Release of silver (Ag) and Copper (Cu) ions

We recorded the release of Ag and Cu ions for the 0.5% Ag@HKUST-1 + FS group on days 1, 2, 4, 21, 30, 60, and 90. Cu ion release was modest on days 1 and 2 but increased significantly between days 4–60, followed by a gradual release until it achieved equilibrium (Figure 11a). There was an increase in the Ag ion release from days 1–20 that stabilized from days 21–30. Then, an increased release of Ag ions was observed between days 31 and 60 followed by a modest release until the 90th day (Figure 11b).

Discussion

MOFs are crystalline porous materials comprised of me-

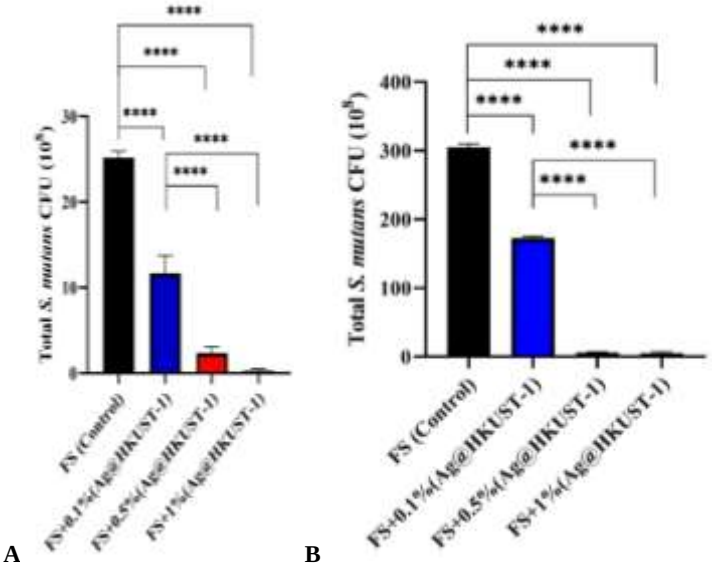

Figure 6: CFU counts of *Streptococcus mutans* (*S. mutans*) biofilm growth with different Ag@HKUST-1 concentrations (0.1%, 0.5% and 1%) after 48 h (a) on the FS surfaces, (b) on the surface of 5% sheep blood agar plates. CFU: Colony forming unit; FS: Fissure sealant; Ag@HKUST-1: Silver (Ag) nanoparticles (NPs) attached to copper-based metal-organic framework (MOF) NPs

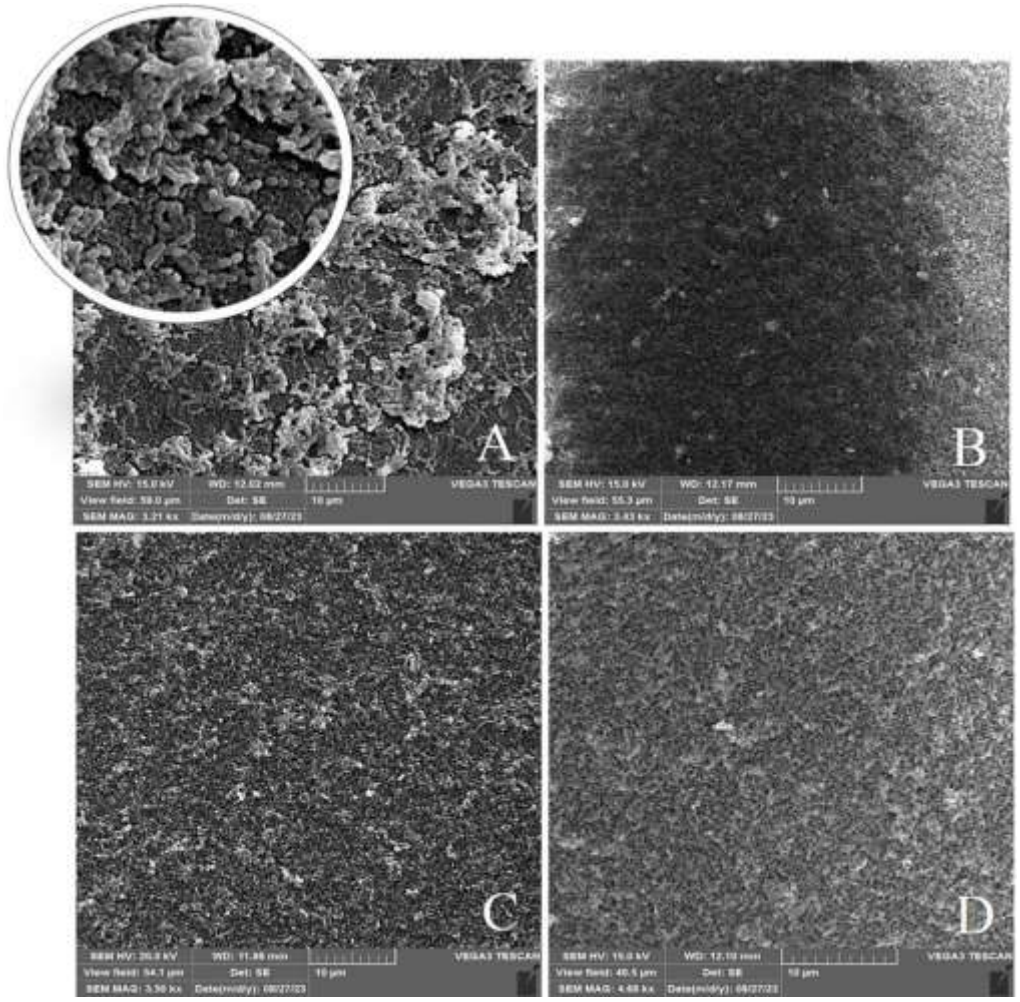

Figure 7: SEM images of *Streptococcus mutans* (*S. mutans*) adhesion on FS discs without NPs and discs that contain different percentages of Ag@HKUST-1. A) FS without NPs (control group), B) FS + 0.1% Ag@HKUST-1, C) FS + 0.5% Ag@HKUST-1, D) FS + 1% Ag@HKUST-1 (magnification: 3210×, 3430×, 3500×, 4680×). SEM: Scanning electron microscope; FS: Fissure sealant; NPs: Nanoparticles; Ag@HKUST-1: Silver (Ag) NPs attached to copper-based metal-organic framework (MOF) NPs

Table 2: Growth of *Streptococcus mutans* (*S. mutans*) after 48h on 5% sheep blood agar in the study groups

CFU	FS	FS + 0.1% Ag@HKUST-1	FS + 0.5% Ag@HKUST-1	FS + 1% Ag@HKUST-1
1/2	$\geq 10^4$	$\geq 10^3$	81	75
1/4	$\geq 10^4$	$\geq 10^3$	44	43
1/8	$\geq 10^3$	900	18	14
1/16	306±3.9	172±2.1	6 ± 0.7	4 ± 1.0

CFU: Colony forming unit ;FS :Fissure sealant; Ag@HKUST-1: Silver (Ag) nanoparticles (NPs) attached to copper-based metal-organic framework (MOF) NPs

Table 3: Failure mode frequency in the study groups

Material	Fracture mode		
	Adhesive	Cohesive	Mixed
FS	1	8	6
FS+0.5% Ag@HKUST-1	2	6	7

FS: Fissure sealant; Ag@HKUST-1: Silver (Ag) nanoparticles (NPs) attached to copper-based metal-organic framework (MOF) NPs

tallic and organic components that have antibacterial properties [20]. The present study is the first to use MOFs in dental materials by incorporating copper-MOF NPs (HKUST-1) into FS. The hydrothermal method was used [9,10] to synthesize these HKUST-1 because of its ability to control the size and shape, and its minimal energy consumption, improved solubility, and formation of thermodynamically stable materials [21] The synthesized HKUST-1 showed an irregular and porous polyhedral structure [12]. Next, we used a protocol by Duan *et al.* [11] to generate Ag@HKUST-1 by adding Ag NPs to the HKUST-1. Various laboratory methods were then used to assess the properties of these NPs. SEM and EDS analyses confirmed the presence of Cu and Ag ions, in addition to uniform dispersion of the Ag NPs throughout the HKUST-1 crystals. XRD spectrum analysis confirmed the presence of Ag on HKUST-1. MOF was used to attach the Ag NPs to prevent their agglomeration. Beery *et al.* [22] found that providing a stable and porous nanoscale base enabled the Ag NPs to

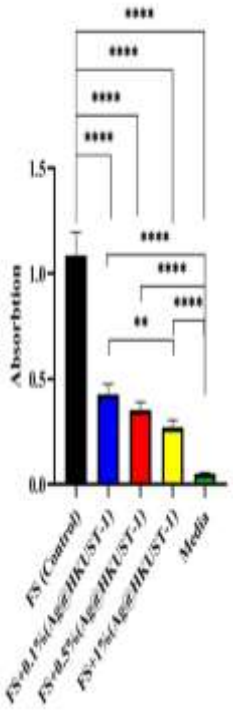

Figure 8: Viability of *Streptococcus mutans* (*S. mutans*) on FS discs with different Ag@HKUST-1 concentrations (0.1%, 0.5% and 1%) assessed by MTT. Medium: Broth culture. FS: Fissure sealants; MTT: 3-(4,5-dimethylthiazol-2-yl)-2, 5-diphenyltetrazolium bromide. FS: Fissure sealant; NPs: Nanoparticles; Ag@HKUST-1: Silver (Ag) NPs attached to copper-based metal-organic framework (MOF) NPs

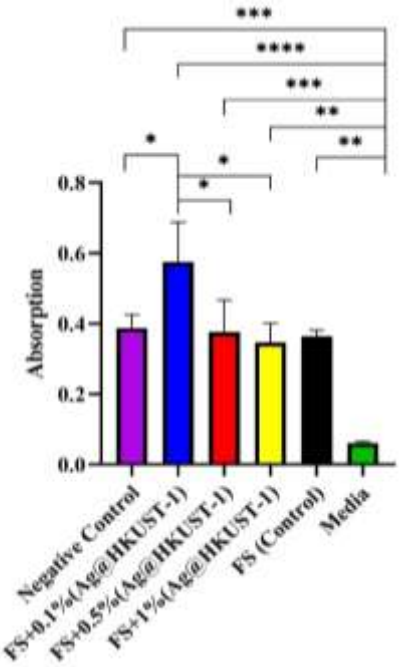

Figure 9: MTT assessment of cytotoxicity of FS without NPs and with 0.1%, 0.5%, and 1% of Ag@HKUST-1 on gingival fibroblast cells. Negative control: Gingival fibroblast cells. Medium: Culture medium without cells. FS: Fissure sealant; Ag@HKUST-1: Silver (Ag) nanoparticles (NPs) attached to copper-based metal-organic framework (MOF) NPs; MTT: 3-(4,5-dimethylthiazol-2-yl)-2, 5-diphenyltetrazolium bromide.

remain stable by stopping oxidation and ion aggregation, and led to prolonged antibacterial properties of the materials, which supported our results.

Antibacterial characteristics of the FS were assessed in different percentages of Ag@HKUST-1 against *S. mutans* biofilms to determine the most effective percentage of Ag. The groups were evaluated by MTT, CFU assessment, CLSM, and SEM [17]. The percentages of NPs chosen were similar to those reported by other researchers [4]. Our findings confirmed the antibacterial properties of Ag@HKUST-1, as reported by others [12].

We chose *S. mutans* because it is a cariogenic, air-tolerant, anaerobic bacteria and the principal cause of dental caries. CLSM and SEM were used to assess bacterial survival and adhesion to the FS surfaces [4,13,14]. Our results demonstrated an inverse correlation between the Ag@HKUST-1 concentration and bacterial adhesion. The antibacterial mechanism is based on the release of Ag and Cu ions, which disrupt the bacterial membrane [5]. Ag ions are gradually released from the HKUST-1 porous network and bind to sulfur-containing proteins in bacterial cell walls. These ions catalyze the production of reactive oxygen species (ROS) within bacterial cells. The ROS induce oxidative stress, which damages bacterial DNA, lipids, and proteins essential for survival and enhances the antimicrobial activity of Ag [23,24]. In the present study, we observed a significant antibacterial effect against *S. mutans* at the 0.5% concentration of Ag@HKUST-1.

It is essential to control the concentration of metal ions because high numbers of metal ions create free radicals, which harm tissue cells [25]. Therefore, we used the MTT test to assess for biocompatibility on human gingival fibroblast cells [14,16]. Our results showed that the different concentrations of NPs in the FS did not cause significant cytotoxicity. Cell survival in the FS with 0.5% Ag@HKUST-1 exceeded 96.52%. Our findings supported those of Zhang *et al.* [26], and Torres-Rosas *et al*. [27] who reported that addition of 0.1% Ag NPs, and 0.01% Cu NPs to dental materials did not have any negative effects on the cells. Aguilar-Perez *et al*. [28] observed that adding 4% Cu NPs to glass ionomer cement did not significantly reduce dental pulp cell viability; we used a lower perce-

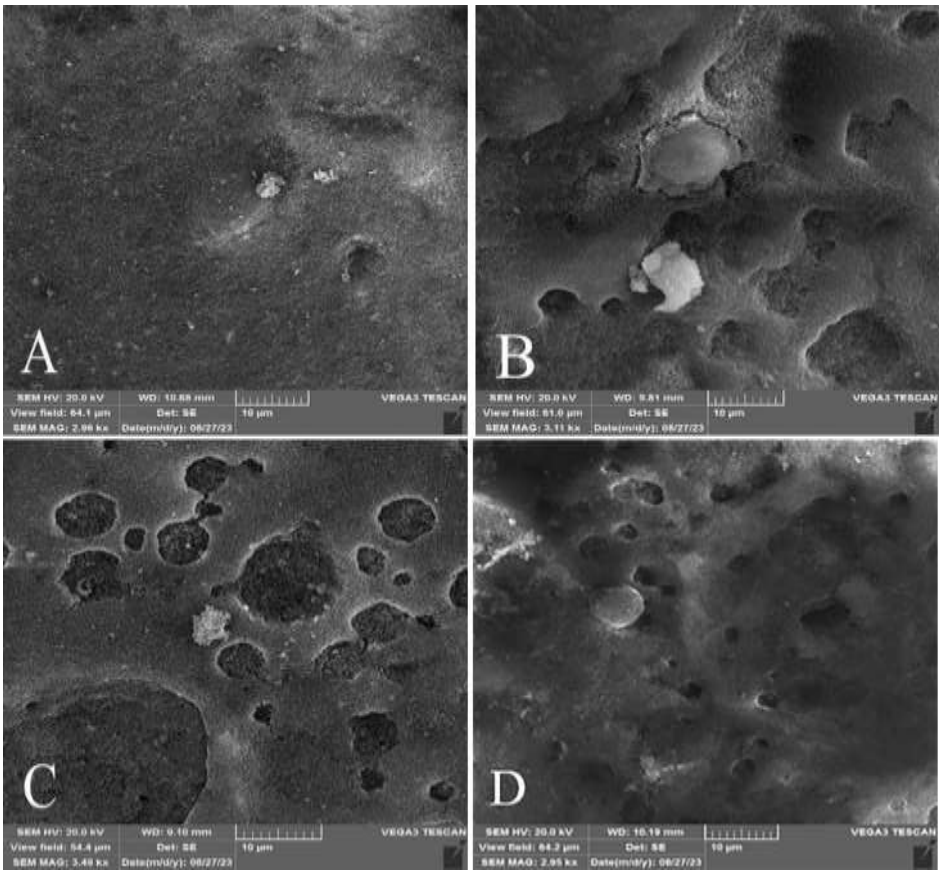

Figure 10: SEM images of fibroblast cell morphology and adhesion, **a:** FS without NPs (control group), **b:** FS+0.1% Ag@HKUST-1, **c:** FS+0.5% Ag@HKUST-1, **d:** FS+1% Ag@HKUST-1 (magnification: 2950×, 3110×, 3490×). SEM: Scanning electron microscope; FS: Fissure sealant; NPs: Nanoparticles; Ag@HKUST-1: Silver (Ag) NPs attached to copper-based metal-organic framework (MOF) NPs

centage than what they reported. The estimated IC50 showed that 4.7% by weight of these NPs and FS could achieve 50% cell survival without toxicity. Our SEM images of cellular shape and adhesion indicated that the porous structure of the Ag@HKUST-1 promoted significant cellular adherence and growth. Their porous shape promotes biocompatibility by improving gingival fibroblast cell interaction, which highlights their potential to aid tissue integration and regeneration [29]. The smooth, uniform surface of the control group did not exhibit these properties. Our bacterial and cellular results indicated that the 0.5% Ag@HKUST-1 was the best choice for physicochemical and mechanical testing.

The depth of cure is appropriate when the resin composite hardness adequately polymerized at a specified depth. Insufficient polymerization in deep layers increases free radicals that may have a cytotoxic effect on dental pulp and reduce its mechanical properties [30]. In the present study, we added Ag NPs to the FS, which increased the depth of cure. Other studies concluded that the larger and more porous NP surfaces allowed higher light frequencies to pass through the materials [13,31]. In contrast, Choi *et al.* [4] reported a decrease after adding zinc NPs to the FS. However, similar to our results, their decreased value fell within the acceptable range of ISO 6874 [19]. MOFs have porosity, low density, and a large surface area [32]. Hence, their use in FS increases light reflection and scattering. Consequently, this may increase the speed of light transmission, its penetration into deeper layers, and the depth of cure.

We observed that adding NPs to resin-based materials increased microhardness, which supported the findings of other studies [13,17,33]. NPs added to the organic phase influence the final filler volume [34]. However, some believe it does not affect microhardness [35]. The differences in findings are mostly due to the percentage and type of NPs.

Low viscosity and high flow are desired for FS. Aziz *et al.* [33] showed that adding 1%–2% NPs led to decreased FS flow. However, Albeshir *et al.* [36] noticed that 20% NPs did not reduce flow composite resin viscosity. We found that the flow of FS with NPs increa-

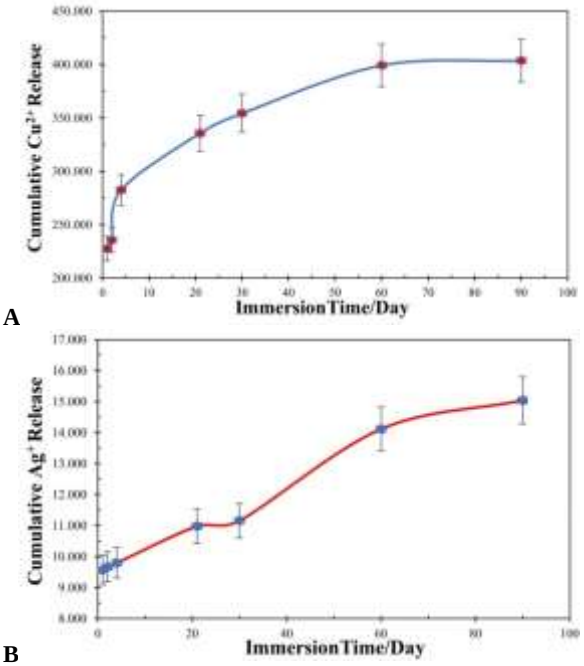

Figure 11: a: Release of copper ions from the 0.5% Ag@HKUST-1 group in DW over time, **b:** Release of Ag ions from the 0.5% Ag@HKUST-1 group in DW over time. Ag: Silver; Ag@HKUST-1: Ag nanoparticles (NPs) attached to copper-based metal-organic framework (MOF) NPs; DW: Deionized water

sed. The difference may be related to the type of structure of the MOFs. This porous polymer has stable pores, larger surface area and organic ligands with hydrophilic property that causes strong binding with functional groups in FS and results in decreased viscosity [31-32].

Our findings showed that the flexural bond strength of NP-associated FS was more than the control, which was in accordance with Marovic *et al.* [37] However, some researchers reported that the differences were not significant [4,13]. The enhanced flexural bond strength may be related to the use of Cu MOFs to assemble the Ag NPs. SEM images revealed an absence of air-bubble and proper links between the NPs and matrix.

Our results showed that the added NPs did not influence SBS, which supported the findings of Fei *et al.* [17] and Zhang *et al*. [26]. In contrast, some reported increased SBS when adding Ag and Cu NPs to resin-based materials [27]. The differences may relate to the tooth type and surface (enamel, dentin), and methods and materials used. Although micromechanical bonding has the main role in bond of composite resin to tooth, a chemical bond between the monomer's hydroxyl/ carboxyl groups and hydroxyapatite may contribute. The NPs have an electric charge; therefore, the probability of creating a hydrogen bond by these particles is weak and would not affect SBS [17,26].

Microleakage at tooth-material interfaces enhances sensitivity, caries, and pulp irritation [38]. Our findings showed some degree of microleakage in both groups, which indicated that the microleakage may be inevitable. Like others, no significant difference was observed between the groups, which showed that the small NP size did not impact the microleakage [18].

We evaluated color changes using a spectrophotometer to measure whiteness [7]. Our data showed the values in both groups were beyond the detectable threshold, which was possibly due to repeated temperature cycling that caused internal stress and water absorption in the materials. After 5000 heat cycles, the 0.5% NPs had a nonsignificant reduction in color change, which was similar to the Hong *et al.* [39] findings. Others believe that Ag NPs cause yellow or brown discoloration of the FS because of rough surfaces from improper NP spread [7]. We used MOFs with low NPs concentrations to prevent NP aggregation and rough surface development.

Ag NPs exhibit antibacterial activity for up to four months [40]. In the current study, the discs were immersed in a new solution after each sampling to improve ion measurement accuracy [41]. Cu ion release increased from days 1 to 60 and Ag ion release increased until day 90 because of penetration into the MOFs pores and slow release. Some studies reported similar linear Ag ion release after 48h and 30 days, respectively [42-43]. Ion release depends on the scaffold solubility, size, shape, and type of NPs [42].

The results of laboratory studies are useful for deciding the appropriate clinical treatment; however, there are limitations with accurate replication of the oral environment. Here, we used thermocycling to mimic oral conditions to decrease this interference [44]. In addition, the research steps followed guidelines for methods procedures and laboratory tests, and were conducted by one operator. The limitation of this study was the lack of comparable prior research, which led to comparisons with the closest available studies. The sample size was also a limitation; therefore, further studies with larger samples and clinical research to assess the properties of this type of FS are recommended.

Conclusion

The FS that contained 0.5% of Ag@HKUST-1 NPs ex-

hibited strong antibacterial properties with minimal cytotoxicity and was comparable to conventional FS in terms of microleakage, SBS and color change. However, it performed better than conventional FS in mechanical properties like depth of cure, microhardness, and flexural bond strength. The sustained release of Cu and Ag ions for 60–90 days suggests the preservation of antibacterial properties, which makes it a suitable alternative to conventional FS.

Acknowledgments

The authors thank the Vice-Chancellory of Research of Shiraz University of Medical Sciences, for supporting this research. This manuscript reports research done in partial fulfillment of the requirements for the PhD degree awarded to one of the authors, Nilofar Mokhtari.

Author contributions

M.M., M.A and A.R.: conceptualized and designed the study, supervised data collection, interpreted the data, drafted the manuscript, and approved the final manuscript as submitted. N.M.: Contributions to conceptualization and design the study, data collection, carried out the initial analyses, reviewed the manuscript, and approved the final manuscript as submitted. All authors agreed to be accountable for all aspects of this work.

Competing interest statement

The authors of this manuscript declare that they have no conflicts of interest.

Funding

This work was supported by vice-chancellery of Shiraz University of Medical Sciences. (Grant No. 28604).

Data availability statement

The datasets generated and/or analyzed during the current study are available from the corresponding author upon reasonable request.

Ethics approval and consent to participate:

The study was approved by the Ethics Review Committee of the School of Dentistry, Shiraz University of Medical Sciences (IR.SUMS.DENTAL.REC.1401.041).

Conflict of Interest

The authors of this manuscript declare that they have no conflicts of interest.

References

[1] Kantovitz KR, Pascon FM, Alonso R, Nobre-Dos-Santos M, Rontani R. Marginal adaptation of pit and fissure sealants after thermal and chemical stress. A SEM study. Am J Dent. 2008; 21: 377-382.

[2] Nedeljkovic I, De Munck J, Slomka V, Van Meerbeek B, Teughels W, Van Landuyt K. Lack of buffering by composites promotes shift to more cariogenic bacteria. J Dent Res. 2016; 95: 875-881.

[3] Swetha DL, Vinay C, Uloopi K, RojaRamya KS, Chandrasekhar R. Antibacterial and mechanical properties of pit and fissure sealants containing zinc oxide and calcium fluoride nanoparticles. Contemp Clin Dent. 2019; 10: 477-482.

[4] Choi JW, Yang SY. Effect of zinc oxide incorporation on the antibacterial, physicochemical, and mechanical properties of pit and fissure sealants. Polymers. 2023; 15: 529.

[5] Malik S, Waheed Y. Emerging applications of nanotechnology in dentistry. Dent J. 2023; 11: 266.

[6] Netalkar PP, Ym K, Natarajan S, Gadipelly T, Bhat P D, Dasgupta A, et al. Effect of nano-hydroxyapatite incorporation on fluoride-releasing ability, penetration, and adaptation of a pit and fissure sealant. Int J Paediatr Dent. 2022; 32: 344-351.

[7] Ferreira I, Alves OL, Schiavon MA, Dos Reis AC. Influence of incorporation of nanostructured silver vanadate decorated with silver nanoparticles on roughness, microhardness, and color change of pit and fissure sealants. Heliyon. 2024; 10: e25525.

[8] Xu VW, Nizami MZI, Yin IX, Yu OY, Lung CYK, Chu CH. Application of copper nanoparticles in dentistry. Nanomaterials. 2022; 12: 805.

[9] Fardjahromi MA, Nazari H, Tafti SA, Razmjou A, Mukhopadhyay S, Warkiani M. Metal-organic framework-ba-sed nanomaterials for bone tissue engineering and wound healing. J Mater Chem. 2022; 23: 100670.

[10] Xiao J, Chen S, Yi J, Zhang HF, Ameer GA. A cooperative copper metal–organic framework-hydrogel system improves wound healing in diabetes. Adv Funct Mater. 2017; 27: 1604872.

[11] Duan C, Meng J, Wang X, Meng X, Sun X, Xu Y, et al. Synthesis of novel cellulose-based antibacterial composites of Ag nanoparticles@ metal-organic frameworks@ carboxymethylated fibers. Carbohydr Poly. 2018; 193: 82-88.

[12] Guo C, Cheng F, Liang G, Zhang S, Jia Q, He L, et al. Copper-based polymer-metal–organic framework embedded with Ag nanoparticles: Long-acting and intelli-

gent antibacterial activity and accelerated wound healing. Chem Engin J. 2022; 435: 134915.

[13] Lai CC, Lin CP, Wang YL. Development of antibacterial composite resin containing chitosan/fluoride microparticles as pit and fissure sealant to prevent caries. J Oral Microbiol. 2022; 14: 2008615.

[14] Yu F, Yu H, Lin P, Dong Y, Zhang L, Sun X, et al. Effect of an antibacterial monomer on the antibacterial activity of a pit-and-fissure sealant. PloS one. 2016; 11: e0162281.

[15] Wang H, Wang S, Cheng L, Jiang Y, Melo MAS, Weir MD, et al. Novel dental composite with capability to suppress cariogenic species and promote non-cariogenic species in oral biofilms. Mater Sci Engineering C. 2019; 94: 587-596.

[16] Cao L, Yan J, Luo T, Yan H, Hua F, He H. Antibacterial and fluorescent clear aligner attachment resin modified with chlorhexidine loaded mesoporous silica nanoparticles and zinc oxide quantum dots. J Mech Biomed Mater. 2023; 141: 105817.

[17] Fei X, Li Y, Weir MD, Baras BH, Wang H, Wang S, et al. Novel pit and fissure sealant containing nano-CaF2 and dimethylaminohexadecyl methacrylate with double benefits of fluoride release and antibacterial function. Dent Mater. 2020; 36: 1241-1253.

[18] Fei X, Li Y, Zhang Q, Tian C, Li Y, Dong Q, et al. Novel pit and fissure sealant with nano-CaF2 and antibacterial monomer: Fluoride recharge, microleakage, sealing ability and cytotoxicity. Dent Mater J. 2024; 43: 346-358.

[19] ISO-6874; Polymer-Based Pit and Fissure Sealants. International Organization for Standardization: Geneva, Switzerland. Available at: https://www.iso.org/obp/ui/#iso:std:iso: 6874:ed-3:v1:en

[20] Li Y, Xia X, Hou W, Lv H, Liu J, Li X. How effective are metal nanotherapeutic platforms against bacterial infections? A comprehensive review of literature. Int J Nanomedicine. 2023; 18: 1109-1128.

[21] Ediati R, Dewi S, Hasan M, Kahardina M, Murwani I, Nadjib M. Mesoporous HKUST-1 synthesized using solvothermal method. Rasayan J Chem. 2019; 12: 1653-1659.

[22] Beery D, Mottaleb MA, Meziani MJ, Campbell J, Miranda IP, Bellamy M. Efficient route for the preparation of composite resin incorporating silver nanoparticles with enhanced antibacterial properties. Nanomaterials. 2022; 12: 471.

[23] Das B, Dash SK, Mandal D, Ghosh T, Chattopadhyay S, Tripathy S, et al. Green synthesized silver nanoparticles destroy multidrug resistant bacteria via reactive oxygen species mediated membrane damage. Arabian J Chem. 2017; 10: 862-876.

[24] Song Z, Wu Y, Wang H, Han H. Synergistic antibacterial effects of curcumin modified silver nanoparticles through ROS-mediated pathways. Mater Sci Eng C Mater Biol Appl. 2019; 99: 255-263.

[25] Xiao J, Zhou Y, Ye M, An Y, Wang K, Wu Q, et al. Freeze-thawing chitosan/ions hydrogel coated gauzes releasing multiple metal ions on demand for improved infected wound healing. Adv Healthc Mater. 2021; 10: 2001591.

[26] Zhang K, Li F, Imazato S, Cheng L, Liu H, Arola DD, et al. Dual antibacterial agents of nano-silver and 12-methacryloyloxydodecylpyridinium bromide in dental adhesive to inhibit caries. J Biomed Mater Res B Appl Biomater. 2013; 101: 929-938.

[27] Torres-Rosas R, Torres-Gómez N, García-Contreras R, Scougall-Vilchis RJ, Domínguez-Díaz LR, Argueta-Figueroa L. Copper nanoparticles as nanofillers in an adhesive resin system: An in vitro study. Dent Med Problems. 2020; 57: 239-246.

[28] Aguilar-Perez D, Vargas-Coronado R, Cervantes-Uc JM, Rodriguez-Fuentes N, Aparicio C, Covarrubias C, et al. Antibacterial activity of a glass ionomer cement doped with copper nanoparticles. Dent Mater J. 2020; 39: 389-396.

[29] Yao X, Chen X, Sun Y, Yang P, Gu X, Dai X. Application of metal-organic frameworks-based functional composite scaffolds in tissue engineering. Regen Biomater. 2024; 11: rbae009.

[30] AlShaafi MM. Factors affecting polymerization of resin-based composites: A literature review. Saudi Dent J. 2017; 29: 48-58.

[31] Marovic D, Par M, Tauböck TT, Haugen HJ, Negovetic Mandic V, Wüthrich D, et al. Impact of copper-doped mesoporous bioactive glass nanospheres on the polymerisation kinetics and shrinkage stress of dental resin composites. Int J Mol Sci. 2022; 23: 8195.

[32] Zhu QL, Xu Q. Metal–organic framework composites. Chem Soc Rev. 2014; 43: 5468-54512.

[33] Aziz S, Javed R, Nowak A, Liaqat S, Khan ZUH, Ahmad N, et al. Effects of TiO2, Ag-TiO2, and Cu-TiO2 nanoparticles on mechanical and anticariogenic properties of

conventional pit and fissure sealants. Open Nano. 2023; 14: 100185.

[34] Gutiérrez MF, Malaquias P, Hass V, Matos TP, Lourenço L, Reis A, et al. The role of copper nanoparticles in an etch-and-rinse adhesive on antimicrobial activity, mechanical properties and the durability of resin-dentine interfaces. J Dent. 2017; 61: 12-20.

[35] Moradian M, Abbasfard D, Jowkar Z. The effect of nanohydroxyapatite and silver nanoparticles on the microhardness and surface roughness of composite resin. General Dent. 2019; 67: 68-71.

[36] Albeshir EG, Balhaddad AA, Mitwalli H, Wang X, Sun J, Melo MAS, et al. Minimally-invasive dentistry via dual-function novel bioactive low-shrinkage-stress flowable nanocomposites. Dent Mate. 2022; 38: 409-420.

[37] Marovic D, Haugen HJ, Negovetic Mandic V, Par M, Zheng K, Tarle Z, et al. Incorporation of copper-doped mesoporous bioactive glass nanospheres in experimental dental composites: Chemical and mechanical characterization. Materials. 2021; 14: 2611.

[38] Asselin M-E, Fortin D, Sitbon Y, Rompre PH. Marginal microleakage of a sealant applied to permanent enamel: evaluation of 3 application protocols. Pediatr Dent. 2008; 30: 29-33.

[39] Hong Q, Pierre-Bez AC, Kury M, Curtis ME, Hiers RD, Esteban Florez FL, et al. Shear bond strength and color stability of novel antibacterial nanofilled dental adhesive resins. Nanomaterials. 2022; 13: 1.

[40] Yin IX, Zhang J, Zhao IS, Mei ML, Li Q, Chu CH. The antibacterial mechanism of silver nanoparticles and its application in dentistry. Int J Nanomedicine. 2020; 15: 2555-2562.

[41] Rodrigues MC, Chiari MD, Alania Y, Natale LC, Arana-Chavez VE, Meier MM, et al. Ion-releasing dental restorative composites containing functionalized brushite nanoparticles for improved mechanical strength. Dent Mater. 2018; 34: 746-755.

[42] Mokabber T, Cao H, Norouzi N, Van Rijn P, Pei Y. Antimicrobial electrodeposited silver-containing calcium phosphate coatings. ACS Appl Mater Interfaces. 2020; 12: 5531-541.

[43] Ai M, Du Z, Zhu S, Geng H, Zhang X, Cai Q, et al. Composite resin reinforced with silver nanoparticles–laden hydroxyapatite nanowires for dental application. Dent Mater. 2017; 33: 12-22.

[44] Fabris D, Souza JC, Silva FS, Fredel M, Gasik M, Henriques B. Influence of specimens' geometry and materials on the thermal stresses in dental restorative materials during thermal cycling. J Dent. 2018; 69: 41-48.